

Forward-backward asymmetry in top quark production from light colored scalars in $SO(10)$ model

Ketan M. Patel^a and Pankaj Sharma^b

Physical Research Laboratory, Navarangpura, Ahmedabad 380 009, India

Abstract

The forward-backward asymmetry in top pair production at Tevatron has been reconfirmed by the CDF collaboration with 5.3 fb^{-1} of accumulated data. These measurements also report that the asymmetry is the largest in regions of high invariant mass $M_{t\bar{t}}$ and rapidity difference $|\Delta Y|$. We consider light colored sextet scalars appearing in a particular non-supersymmetric $SO(10)$ grand unification model within the $\overline{126}$ scalar representation. These scalar states have masses in the range of $300 \text{ GeV} - 2 \text{ TeV}$ consistent with the requirements of gauge coupling unification and bounds on the proton lifetime. The cross section and the total asymmetry can be simultaneously explained with the contributions of these scalars within 1σ . We find that the simultaneous fitting of the cross section, the total asymmetry and the asymmetries in different rapidity and $M_{t\bar{t}}$ bins gives only a marginal improvement over the SM contribution. We also study various production mechanisms of these colored sextet scalars at the LHC.

^a kmpatel@prl.res.in

^b pankajs@prl.res.in

I. INTRODUCTION

The CDF collaboration had measured the forward-backward asymmetry, A_{FB} , in $t\bar{t}$ pair production in the $t\bar{t}$ rest frame in 2008 at Tevatron with 3.2 fb^{-1} of collected data, as [1]

$$A_{FB} \equiv \frac{N(\cos \theta > 0) - N(\cos \theta < 0)}{N(\cos \theta > 0) + N(\cos \theta < 0)} = 0.193 \pm 0.065(\text{stat}) \pm 0.024(\text{syst}) \quad (1)$$

where θ is the scattering angle of top quark in the $t\bar{t}$ rest frame. This result had been confirmed by D0 collaboration based on 0.9 fb^{-1} of integrated luminosity [2]. They reported $A_{FB} = 0.19 \pm 0.09(\text{stat}) \pm 0.02(\text{syst})$ and $A_{FB} = 0.12 \pm 0.08(\text{stat}) \pm 0.01(\text{syst})$ for exclusive 4-jet and inclusive 4-jet events respectively consistent with CDF results. These measurements have attracted a lot of attention due to more than 2σ deviation from the Standard Model (SM) predicted value of $A_{FB}^{SM} = 0.058 \pm 0.009$ [3]. In the SM, the A_{FB} identically vanishes at leading order (LO). However, at next to leading order (NLO) in QCD, it can arise from (a) the interference between tree level SM amplitude and the box diagram, (b) radiative corrections to $q\bar{q}$ annihilation and (c) interference between different amplitudes contributing to gluon-quark scattering. Several independent New Physics (NP) scenarios have been advanced [4–9] to explain this discrepancy.

Recently, CDF have presented new results using 5.3 fb^{-1} of data sets in which A_{FB} is reported to be 0.158 ± 0.074 (stat+syst). Along with this new value of A_{FB} , they find interesting dependences of A_{FB} on the invariant mass of the $t\bar{t}$ pair and their rapidity dependence. The asymmetry is more prominent in the large invariant mass region of $M_{t\bar{t}} > 450 \text{ GeV}$ with more than 3σ deviation and in the large rapidity difference $|\Delta Y| > 1$ region with around 2σ deviation from the SM predicted value [10]. On the other hand, some other observables related to $t\bar{t}$ pair production at Tevatron show good agreement with the SM predicted values. The measured parton level $t\bar{t}$ -pair production cross section $\sigma_{t\bar{t}}^{exp} = 7.70 \pm 0.52$ [11] agrees with the SM predicted value of $\sigma_{t\bar{t}}^{SM} = 7.45^{+0.72}_{-0.63}$ calculated with MCFM [12]. Similarly the experimentally measured invariant mass distribution is also consistent with the prediction of the SM at NLO [13]. Hence, while discussing the new physics scenarios to explain the new results, namely the mass and rapidity dependence of A_{FB} , they must not introduce large corrections to either the total $t\bar{t}$ cross section $\sigma_{t\bar{t}}$ or the invariant mass distribution $M_{t\bar{t}}$. Some recent attempts [14, 15] have been made in order to explain these new observables along with the updated measurements of A_{FB} and $\sigma_{t\bar{t}}$.

The standard model gauge structure ($SU(3)_c \times SU(2)_L \times U(1)_Y$) allows a finite number of different representations of scalar particles which can couple an up or down quark to the top quark. The possible cases include a set of colored octet, singlet, triplet and sextet scalars each for $u\bar{u} \rightarrow t\bar{t}$ and $d\bar{d} \rightarrow t\bar{t}$ processes.

$$\begin{array}{lll} (8, 2, \frac{1}{2}), & (1, 2, \frac{1}{2}), & (\bar{3}, 3, \frac{1}{3}), & (6, 3, \frac{1}{3}) & \text{for } u\bar{u}/d\bar{d} \rightarrow t\bar{t} \\ & (\bar{3}, 1, \frac{4}{3}), & (6, 1, \frac{4}{3}) & & \text{for } u\bar{u} \rightarrow t\bar{t} \text{ only} \\ & (\bar{3}, 1, \frac{1}{3}), & (6, 1, \frac{1}{3}) & & \text{for } d\bar{d} \rightarrow t\bar{t} \text{ only} \end{array} \quad (2)$$

The effects of these scalars on A_{FB} have been studied in a model independent way in several papers. For example, the results of Shu *et al* [5] show that colored sextet and triplet scalars are able to explain the anomaly while the analysis of Jung *et al* [6] favours the singlets and sextets. On the other hand, the results of Arhrib *et al* [7] show that sextet diquarks could not fit the A_{FB} and cross section simultaneously within 1σ . However all these analyses were based on old observations of A_{FB} . According to the new CDF data, the central value of A_{FB} has significantly come down. Also the distributional preferences of A_{FB} in invariant mass and rapidity have been reported. So it is an interesting exercise to study these scalars in the light of new observations. In the present study we investigate the light colored sextet scalars appearing in a well motivated $SO(10)$ grand unified theories as a possible explanation of A_{FB} as well as new observables simultaneously based on current data.

Colored scalar fields naturally emerge in a well motivated class of grand unified theories. For example, the representations $(8, 2, \frac{1}{2})$ and $(\bar{3}, 1, \frac{4}{3})$ reside in a 45-dimensional Higgs field of $SU(5)$. It is interesting to note that in any simple renormalizable version of non-supersymmetric $SU(5)$, the 45 Higgs together with 5-dimensional Higgs is necessarily required to generate viable masses of charged fermions [16]. It has been shown through detailed studies in reference [8, 9] that both the scalar states $(8, 2, \frac{1}{2})$ and $(\bar{3}, 1, \frac{4}{3})$ can have masses in the range of 300 GeV - 1 TeV consistent with the requirements of gauge coupling unification and bound on the proton lifetime. In addition, the contribution of colored triplet scalar to the production of $t\bar{t}$ at the Tevatron can enhance the forward-backward asymmetry and account for the experimental result without spoiling the successful standard model prediction for the total cross section. We investigate a similar possibilities in more predictive and attractive class of grand unified theories based on the $SO(10)$ gauge group. The remarkable feature of $SO(10)$ is that its 16-dimensional irreducible spinor representation accommodates a complete family of fermions, including the right-handed neutrino. This complete unification of quarks and leptons opens up the possibly of connections between the charge fermions and the neutrino sector. Furthermore, $SO(10)$ has the left-right symmetry group $SU(2)_L \times SU(2)_R$ as a subgroup, making the implementation of the both the type-I and the type-II seesaw mechanisms very natural in these theories. The 45 dimensional scalar representation of $SU(5)$ resides in both the $\overline{126}$ and the 120 dimensional scalar representations of $SO(10)$ which can couple with ordinary fermions through the Yukawa interactions. The $\overline{126}$ Higgs field plays an important role in gauge symmetry breaking [17] as well as it is essential for viable fermion masses [18]. However the color triplets of $\overline{126}$ couple with fermions through symmetric leptoquark couplings and can induce the rapid proton decay if assumed light. On the other hand, the 120 Higgs field has antisymmetric coupling with fermions but it is not required if one sticks to the minimal Higgs content of the theory. We show in this work that the $\overline{126}$ Higgs has diquark colored sextets and octets at TeV scale consistent with gauge coupling unification and proton decay bounds and study the role of the sextet scalars as the possible candidates to explain the anomaly in $t\bar{t}$ production observables.

This paper is organized as follows. In the next section, we study the scalar spectrum of a

particular $SO(10)$ model and discuss the constraints coming from gauge coupling unification and proton decay. In section III, we study the role of light colored sextet scalars on the $t\bar{t}$ pair production observables. In section IV, we will study the signatures of these scalars at both 7 TeV and 14 TeV LHC. Finally, we summarize our results in section V.

II. LIGHT COLORED SCALARS IN $SO(10)$ MODEL

We consider non-supersymmetric $SO(10)$ as a basic framework of our model. It has been pointed out in recent studies [17] that an adjoint 45-dimensional scalar representation (χ) of $SO(10)$ together with one $\overline{16}$ or $\overline{126}$ (Σ) Higgs can govern the entire breaking of $SO(10)$ gauge symmetry down to the SM. If one sticks to the renormalizable version of the seesaw mechanisms then the representation $\overline{126}$ is indispensable, since it breaks the $SU(2)_R$ group and gives neutrino masses through seesaw mechanisms. In addition, one needs 10 dimensional Higgs (ϕ) to obtain a realistic fermion mass spectrum [18]. We have given the decompositions and full SM spectrum of these scalar fields in Table IV in Appendix. Note that χ contains two SM singlets (χ_3, χ_8) and Σ contains one (Σ_9) SM singlet that acquire vevs at GUT scale and break $SO(10)$ to the SM group. The 10 and $\overline{126}$ Higgs contain the SM doublets ($\phi_2, \bar{\phi}_2$) and ($\Sigma_2, \bar{\Sigma}_2$) respectively which can mix through a renormalizable term $\chi_{ij}\chi_{kl}\Sigma_{ijklm}\phi_m$ in the scalar potential. For consistent fermion mass spectrum, one has to keep (at least) one linear combination of these doublets light upto the electroweak scale, which plays the role of SM Higgs doublet and triggers the electroweak symmetry breaking. This requires a fine tuning in the parameters of the Higgs potential. Assuming such fine tuning in parameters, a detailed numerical analysis has been carried out recently for viable fermion mass spectrum in this model in Ref. [18]. It has been shown that such model can provide very predictive structure of fermion masses if a global $U(1)_{PQ}$ (Peccei-Quinn) symmetry is imposed and can produce realistic fermion mass spectrum which is in excellent agreement with the present data extrapolated at the GUT scale.

We consider a non-supersymmetric $SO(10)$ framework with the minimal Higgs fields $10 + 45 + \overline{126}$ in our attempt to explain the forward-backward asymmetry in $t\bar{t}$ production at Tevatron. Following previous studies, we assume that only one linear combination of the weak doublets of 10 and $\overline{126}$ remains light and becomes the SM Higgs. Further, we also need to assume that the scalar submultiplets which can potentially contribute to the asymmetry in the production of top quarks also remain light in the range of 300 GeV - 2 TeV. Among the possible options allowed by the SM gauge symmetry shown in Eq. 2, the $\overline{126}$ contains three sextets $\Sigma_3(6, 1, \frac{4}{3})$, $\Sigma_4(6, 1, \frac{1}{3})$, $\Sigma_{12}(\bar{6}, 3, -\frac{1}{3})$ and a pair of octets $\Sigma_{15}(8, 2, \frac{1}{2})$, $\bar{\Sigma}_{15}(8, 2, -\frac{1}{2})$. These fields couple to the 16-plet matter through Yukawa interactions. Furthermore, all these fields are diquark (have only quark-quark coupling) in nature and do not mediate the proton decay. Some other components of the $\overline{126}$ scalar (like Σ_1, Σ_7 and Σ_{13}) also have the correct quantum numbers to influence $t\bar{t}$ production but they have leptoquark coupling which induce rapid proton decay if assumed light. If no artificial suppression via Yukawa couplings is arranged their masses should not be below than 10^{12} GeV due to proton decay

constraints.

The interaction of $\overline{126}$ Higgs field to the 16-dimensional matter fields ψ can be written in its most general form as [19]

$$-\mathcal{L}_Y = \frac{1}{5!} F_{ij} \psi_i^T \mathcal{B} C^{-1} \Gamma_p \Gamma_q \Gamma_r \Gamma_s \Gamma_t \psi_j \Sigma_{pqrst} \quad (3)$$

where the indices i, j denote family indices, $p, q, \dots = 1, \dots, 10$ are $SO(10)$ indices, C is the Dirac charge conjugation matrix and $\mathcal{B} = \Gamma_1 \Gamma_3 \Gamma_5 \Gamma_7 \Gamma_9$ is the equivalent of the charge conjugation matrix for $SO(10)$ that ensures the invariance under $SO(10)$. Γ_i 's are representations of the Clifford algebra associated with the Lie algebra of the $SO(10)$ group and are given in [19, 20]. F is the Yukawa coupling matrix and it is symmetric by its $SO(10)$ properties. After the decomposition [21] of Eq. 3, the couplings of Σ_3 , Σ_4 , Σ_{12} and Σ_{15} to matter can be written as

$$\begin{aligned} -\mathcal{L}_Y \ni & -2F_{ij} u_{ai}^{CT} C^{-1} u_{bj}^C \Sigma_{3ab}, \\ & \sqrt{2} F_{ij} u_{ai}^{CT} C^{-1} d_{bj}^C \Sigma_{4ab}, \\ & -2F_{ij} Q_{ai}^T C^{-1} \varepsilon \Sigma_{12ab} Q_{bj}, \\ & -2F_{ij} (u_{ai}^T (T^A)_{ab} C^{-1} u_{bj}^C \Sigma_{15}^{0A} + d_{ai}^T (T^A)_{ab} C^{-1} u_{bj}^C \Sigma_{15}^{+A}) \\ & \sqrt{2} F_{ij} (d_{ai}^T (T^A)_{ab} C^{-1} d_{bj}^C \bar{\Sigma}_{15}^{0A} + u_{ai}^T (T^A)_{ab} C^{-1} d_{bj}^C \bar{\Sigma}_{15}^{-A}) \end{aligned} \quad (4)$$

where $T^A = \frac{1}{2} \lambda^A$ and λ^A ($A = 1, \dots, 8$) are the Gell-Mann matrices of $SU(3)$. a, b, c are color indices. Clearly, all these fields have the right couplings to influence the asymmetry we are interested in. However, in order to be relevant for asymmetry at Tevatron, all these fields or at least one of them must be sufficiently light. On the other hand, such light states will contribute to the running of gauge couplings and hence viability of their being light is constrained by the unification of gauge couplings and present bound on the proton lifetime. We thus show that it is possible to achieve light colored scalars with successful gauge coupling unification in a consistent way in our model.

In the absence of any new particle thresholds between the weak and GUT scales, the running of gauge couplings at one-loop level is given by

$$\alpha_{GUT}^{-1} = \alpha_i^{-1}(M_Z) - \frac{b_i}{2\pi} \ln \left(\frac{M_{GUT}}{M_Z} \right) \quad (5)$$

where α_{GUT} represents the gauge coupling at the unification scale M_{GUT} . b_i 's are the appropriate one-loop β function coefficients [22] and $i = 1, 2, 3$ stands for $U(1)_Y$, $SU(2)_L$ and $SU(3)_c$ respectively. Their values for the SM with one light Higgs doublet are $b_1 = \frac{41}{10}$, $b_2 = -\frac{19}{6}$ and $b_3 = -7$. It is easy to check that these values for b_i do not unify the gauge couplings since SM does not predict gauge coupling unification in the first place. The presence of new particles between weak and GUT scale can change the running and it can be easily incorporated by replacing b_i in Eq. 5 with effective one-loop coefficients B_i defined by [23]

$$B_i = b_i + \sum_I b_{iI} \frac{\ln(M_{GUT}/M_I)}{\ln(M_{GUT}/M_Z)} \quad (6)$$

where b_{iI} is the one-loop coefficient of the additional particle I of mass M_I lying between M_Z and M_{GUT} . Following Giveon *et al.* [23], Eq. 5 with contributions from Eq. 6 can provide successful gauge coupling unification at one loop level if they satisfy following two conditions:

$$\frac{B_{23}}{B_{12}} \equiv \frac{B_2 - B_3}{B_1 - B_2} = \frac{5 \sin^2 \theta_W - \alpha/\alpha_s}{8 \cdot 3/8 - \sin^2 \theta_W} = 0.716 \pm 0.005 \quad (7)$$

$$B_{12} \equiv B_1 - B_2 = \frac{16\pi}{5\alpha} \frac{3/8 - \sin^2 \theta_W}{\ln(M_{GUT}/M_Z)} = \frac{184.9 \pm 0.2}{\ln(M_{GUT}/M_Z)} \quad (8)$$

We use the present experimental measurements of the SM parameters [24] to derive the above numbers. In any given model, B_{ij} depend only on the particle content and associated mass spectrum and conditions (7) allow us to constrain the mass spectrum of particles that leads to an exact unification at GUT scale. We give a list of the different submultiplets of 10, $\overline{126}$ and 45 scalar representations and the corresponding contributions to coefficients B_{ij} in Table(IV) in the Appendix.

In order to present a consistent analysis, we now discuss the constraints coming from proton decay. In nonsupersymmetric GUTs, this process is mediated by baryon number violating gauge interactions which induce a set of effective dimension six operators at low energies that conserve $B - L$. In the $SO(10)$ scenario we consider here, such gauge bosons are integrated out at the GUT scale ($m_{X,Y} = M_{GUT}$) and therefore proton decay constrains M_{GUT} from below. The most stringent bounds coming from the latest experimental limit on partial decay lifetime of proton τ_p ($p \rightarrow \pi^0 e^+$) $> 8.2 \times 10^{33}$ years [25] implies

$$M_{GUT} \approx (m_p^5 \alpha_{GUT}^2 \tau_p)^{\frac{1}{4}} \gtrsim 2.3 \times 10^{16} \sqrt{\alpha_{GUT}} \text{ GeV}, \quad (9)$$

where $m_p = 0.938$ GeV is the proton mass. Some of the submultiplets of 10 and $\overline{126}$ Higgs are leptoquark scalars (for example, $\phi_1, \Sigma_1, \Sigma_6$ and etc.) and are associated with $d = 6$ proton decay operators. We suppress their contribution to proton decay by making them super heavy $\sim M_{GUT}$ as we will explain in next paragraph.

As mentioned earlier in this section, it is necessary that at least one of the submultiplets ($\Sigma_3, \Sigma_4, \Sigma_{12}$ and Σ_{15}) of $\overline{126}$ remains light in order to explain the forward-backward asymmetry in top quark production. Typically in theories with two or more widely different mass scales, if a submultiplet of a full Higgs multiplet acquires a vev $\simeq M$, the members of that multiplet acquire a mass $\sim M$ [26]. Any scenario which differs from this would require some fine tunings in the parameters of the scalar potential. To check the viability of such fine tunings, a complete detailed analysis of scalar potential minimization and its diagonalization is required. However this is beyond the scope of present work and we assume that such fine tuning is possible in our case. In order to avoid further unnecessary fine tunings, we assume that the remaining submultiplets of the scalar fields 10, 45, $\overline{126}$ are super heavy and have natural masses of order M_{GUT} . In other words, we assume that only those submultiplets of scalar fields remain light and have masses M_I in between the weak scale and the GUT scale and may potentially contribute to the forward-backward asymmetry in $t\bar{t}$ production.

With all these considerations, we now check the compatibility of light colored scalar states of our interest with the unification of the gauge couplings and constraints on GUT scale coming from proton decay bounds. Following the strategy of [8], we determine an upper bound on GUT scale at the one loop level assuming that any one of $\Sigma_3, \Sigma_4, \Sigma_{12}$ and Σ_{15} is responsible for asymmetry and is accordingly in the mass range of 300 GeV - 2 TeV. For this, we numerically maximize M_{GUT} while imposing the condition that the solution satisfies Eq. 7. The additional constraints we put on the solution are $300 \text{ GeV} \leq m_{\Sigma_3}, m_{\Sigma_4}, m_{\Sigma_{12}}, m_{\Sigma_{15}} = m_{\bar{\Sigma}_{15}} \leq M_{GUT}$ and $M_{GUT} \leq M_{Planck} = 10^{19} \text{ GeV}$. The results of our numerical analysis are shown in Fig. 1 and Fig. 2. We get viable gauge coupling unification consistent with proton decay limits in two different scenarios.

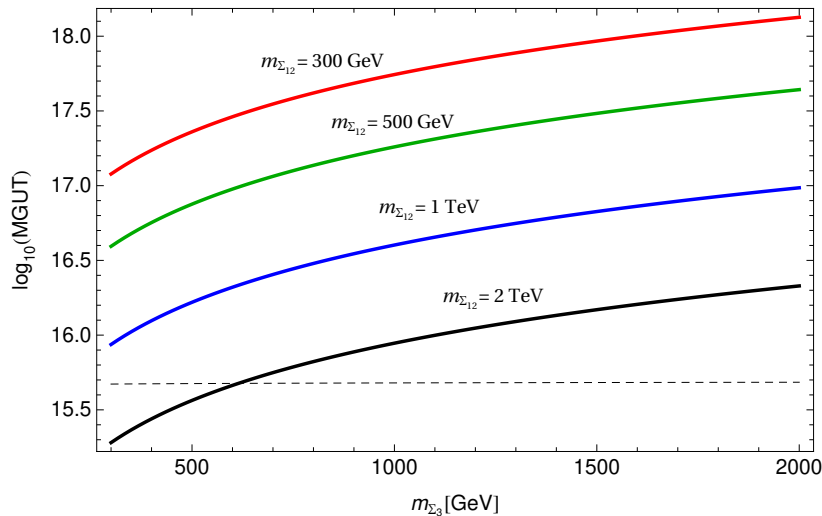


FIG. 1. The maximum value of M_{GUT} obtained for different values of $m_{\Sigma_{12}}$ by assuming Σ_3 light. The dashed line stands for the lower bound on M_{GUT} due to the proton lifetime. Viable gauge coupling unification is achieved in the region between $m_{\Sigma_{12}}=300 \text{ GeV}$ and the dashed line.

(A) We get successful gauge coupling unification for the scalar diquark Σ_3 having mass in the range of 300 GeV to 2 TeV as shown in Fig. 1. The light Σ_3 also requires light $\Sigma_{12}(\bar{6}, 3, -\frac{1}{3})$ and there is a clear correlation between their masses. There exists an upper bound on $m_{\Sigma_{12}}$ for a given value of m_{Σ_3} . For example, when $m_{\Sigma_3} = 600 \text{ GeV}$ we have $m_{\Sigma_{12}} \leq 2 \text{ TeV}$. The other two scalar states remain heavy, namely, $\Sigma_{15} \sim 10^9 - 10^{12} \text{ GeV}$ and $\Sigma_4 \sim M_{GUT}$.

(B) Unification of gauge coupling is also achieved with light sextet diquark state $\Sigma_4(6, 1, \frac{1}{3})$ as shown in Fig. 2. Unlike light Σ_3 in the previous case it does not require any other light submultiplet at TeV scale. The maximum value of the GUT scale does not change appreciably with m_{Σ_4} and stays well above the present proton decay limits shown by the dashed line in Fig. 2. Successful unification in this case requires only one state at intermediate scale $m_{\Sigma_{12}} \sim 10^8 \text{ GeV}$ and Σ_3, Σ_{15} and remain superheavy ($\sim M_{GUT}$).

From the results of the detailed analysis carried out in this section, we conclude that either Σ_3 or Σ_4 can remain light and influence the forward-backward asymmetry in $t\bar{t}$ production through the processes $u\bar{u} \rightarrow t\bar{t}$ and $d\bar{d} \rightarrow t\bar{t}$ respectively. We do not get viable gauge coupling

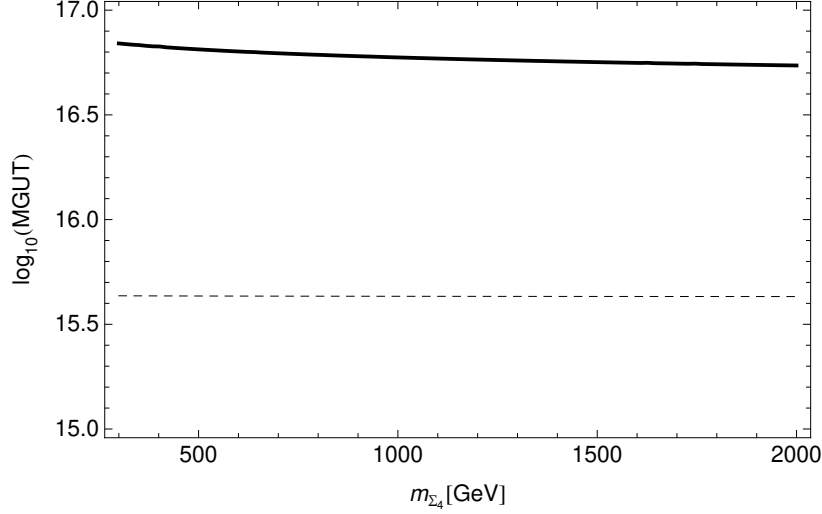


FIG. 2. The maximum value of M_{GUT} obtained by assuming Σ_4 light. The dashed line stands for the lower bound on M_{GUT} due to the proton lifetime. Viable gauge coupling unification is achieved in the region between two lines.

unification with a light colored octet state Σ_{15} and hence this case will be ignored in further analysis. Note that we have presented consistent unification analysis at the one loop level. The allowed masses of Σ_3 and Σ_4 would change slightly if one considers two-loop effects in the running of gauge couplings. However they would still remain within the TeV range.

III. COLORED SEXTETS AND FORWARD-BACKWARD ASYMMETRY OF TOP QUARKS

The light colored sextet scalars Σ_3 and Σ_4 contribute to $t\bar{t}$ pair production through u-channel exchange as shown in Fig. 3. Σ_3 interferes with the SM contributions for $u\bar{u}$ and $c\bar{c}$ initial parton states while Σ_4 interferes with the SM contributions for $d\bar{d}$, $s\bar{s}$ and $b\bar{b}$ initial parton states. The contributions of initial parton states $c\bar{c}$, $s\bar{s}$ and $b\bar{b}$ to the overall process $p\bar{p} \rightarrow t\bar{t}$ will be suppressed due to their small parton distribution functions (PDF). However we include all these contributions in our analysis.

Let us denote incoming quark momentum by p_q , incoming anti-quark momentum by $p_{\bar{q}}$, outgoing top momentum by p_t and outgoing anti-top momentum by $p_{\bar{t}}$ with the following definitions :

$$p_{q,\bar{q}} = \frac{\sqrt{\hat{s}}}{2}(1, 0, 0, \pm 1), \quad (10)$$

$$p_{t,\bar{t}} = [E_t, \pm |\vec{p}_t|(\sin \theta, 0, \cos \theta)], \quad (11)$$

$$\equiv E_t[1, \pm \beta_t(\sin \theta, 0, \cos \theta)] \quad (12)$$

where $E_t = \sqrt{\hat{s}}/2$, $\beta_t = |\vec{p}_t|/E_t \equiv \sqrt{1 - 4m_t^2/\hat{s}}$ and θ is the angle between momenta of the incoming quark and the outgoing top quark in the center of mass (cm) frame of the partons.



FIG. 3. Contributions from light sextet scalars to the $t\bar{t}$ production at the Tevatron.

Neglecting masses of all quarks except the top, the Mandelstam variables in parton cm are defined as follows :

$$\hat{s} = (p_q + p_{\bar{q}})^2 = (p_t + p_{\bar{t}})^2 = x_1 x_2 s, \quad (13)$$

$$\hat{t} = (p_q - p_t)^2 = (p_{\bar{q}} - p_{\bar{t}})^2 = m_t^2 - \frac{\hat{s}}{2}(1 - \beta_t \cos \theta), \quad (14)$$

$$\hat{u} = (p_q - p_{\bar{t}})^2 = (p_{\bar{q}} - p_t)^2 = m_t^2 - \frac{\hat{s}}{2}(1 + \beta_t \cos \theta) \quad (15)$$

where s is the cm energy of proton and antiproton in laboratory frame, x_1 and x_2 are the fractions of momentum carried by the partons inside proton and antiproton respectively.

With these notations and conventions, the matrix amplitude squared (averaged and summed over initial and final color and spin indices respectively) for $(q\bar{q} \rightarrow t\bar{t})$ can be written as follows :

$$\begin{aligned} \overline{\sum} |\mathcal{M}_{total}|^2 &= \frac{2g_s^4}{9} \left[1 + \frac{4m_t^2}{\hat{s}} \sin^2 \theta + \cos^2 \theta \right] \\ &\quad - \frac{4g_s^2}{9} \frac{|f_{13}^{u,d}|^2}{\hat{u} - m_{\Sigma_{3,4}}^2} \left[(1 + \beta_t \cos \theta)^2 + \frac{4m_t^2}{\hat{s}} \right] \\ &\quad + \frac{|f_{13}^{u,d}|^4}{12(\hat{u} - m_{\Sigma_{3,4}}^2)^2} (1 + \beta_t \cos \theta)^2, \end{aligned} \quad (16)$$

where f_{13}^u and f_{13}^d are related with the original coupling F_{13} of Eq. 4 by the following relation

$$f_{13}^u = \sqrt{2} f_{13}^d = 2F_{13}. \quad (17)$$

For our numerical study, we have used the leading order PDF sets of CTEQ6L [27] to convolute with the partonic cross section to obtain hadronic cross section. We set our renormalization and factorization scale to $\mu_R = \mu_F = m_t$. The top mass is taken to be $m_t = 172.5$ GeV at which we also evaluate strong coupling $\alpha_s = 0.1085$. We use K -factor of 1.3 to rescale our LO results for $\sigma(t\bar{t})$ to match with NLO QCD prediction [28].

We calculate the total cross section $\sigma(t\bar{t})$, A_{FB} as defined in Eq. 1, as well as A_{FB} in $|\Delta Y| > 1$, $|\Delta Y| < 1$, $M_{t\bar{t}} < 450$ GeV and $M_{t\bar{t}} > 450$ GeV, where $|\Delta Y|$ is the difference

of top and anti-top quark rapidities i.e., $|\Delta Y| = Y_t - Y_{\bar{t}}$ in $t\bar{t}$ rest frame. The present experimentally measured values of all these observables, their values predicted in the SM and corresponding contributions needed from NP are listed in Table I.

Observables	Experimentally Measured Values	SM Contribution	Contribution needed from NP
Cross section	7.70 ± 0.52	$7.45^{+0.72}_{-0.63}$	—
A_{FB}	0.158 ± 0.074	0.058 ± 0.009	0.1 ± 0.083
$A_{FB}(M_{t\bar{t}} > 450\text{GeV})$	0.475 ± 0.112	0.088 ± 0.0013	0.387 ± 0.1133
$A_{FB}(M_{t\bar{t}} < 450\text{GeV})$	-0.116 ± 0.153	0.04 ± 0.006	-0.156 ± 0.159
$A_{FB}(\Delta Y > 1)$	0.611 ± 0.256	0.123 ± 0.018	0.488 ± 0.274
$A_{FB}(\Delta Y < 1)$	0.026 ± 0.118	0.039 ± 0.006	-0.013 ± 0.124

TABLE I. The observables with their experimentally measured values, their values predicted in the SM and corresponding contributions needed from NP. The contributions needed from NP are obtained by subtracting the SM contributions from experimentally measured values.

We perform a χ^2 analysis to simultaneously fit all the observables shown in Table I. For this, we define the following χ^2 function

$$\chi^2 = \sum_{i=1}^6 \left(\frac{P_i - O_i}{\sigma_i} \right)^2, \quad (18)$$

where the sum runs over all the six observable quantities. P_i 's are the theoretically calculated values of these quantities as a function of couplings and masses of scalars in our model and O_i 's are the mean values of these observables. σ_i 's denote 1σ errors in O_i . The χ^2 is numerically minimized to obtain the best fit over all six observables. The more robust statistic to quantify the quality of fit is reduced- χ^2 which is defined as the χ^2/ν where ν is number of degrees of freedom (d.o.f.) in the analysis. For the SM, the value of total χ^2 is 17.26 and the value of χ^2/ν is 2.88.

We now present a detailed numerical analysis for the contributions of Σ_3 and Σ_4 separately.

A. Diquark $(6, 1, \frac{4}{3})$

In Fig. 4, we plot the cross section and the forward backward asymmetry for $t\bar{t}$ production at Tevatron as a function of the coupling f_{13}^u for four different masses of the colored sextet scalar Σ_3 . In showing the contribution from new physics, we subtract the SM contribution from the experimentally measured value of A_{FB} .

From Fig. 4, we see that sextet Σ_3 of mass 300 GeV can barely satisfy both $\sigma^{t\bar{t}}$ and A_{FB} constraints for a very narrow range of coupling f_{13}^u that too at 2σ . For large masses Σ_3 can

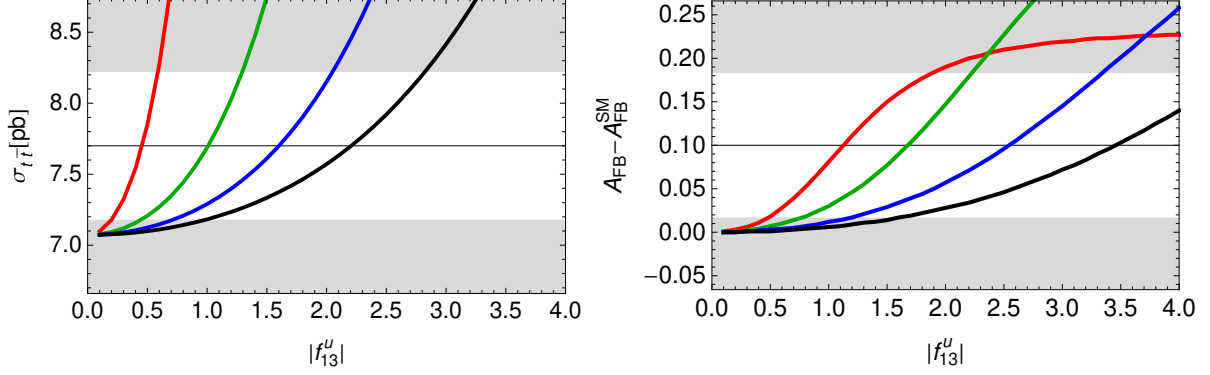


FIG. 4. The $t\bar{t}$ production cross section (left) and the forward backward asymmetry (right) as a function of the coupling f_{13}^u for masses $m_{\Sigma_3} = 300$ GeV (Red), 900 GeV (Green), 1500 GeV (Blue) and 2100 GeV (Black). The unshaded and the shaded region correspond to 1σ and 2σ experimental bounds respectively.

	$m_{\Sigma_3} = 300\text{GeV}$		$m_{\Sigma_3} = 900\text{GeV}$		$m_{\Sigma_3} = 1.5\text{TeV}$		$m_{\Sigma_3} = 2.1\text{TeV}$	
Observables	Fit	pull	Fit	pull	Fit	pull	Fit	pull
Cross section	8.0404	0.6546	8.2761	1.1078	8.3004	1.1546	8.3076	1.1685
A_{FB}	0.0237	-0.919	0.0617	-0.462	0.0690	-0.3729	0.0715	-0.3429
$A_{FB}(M_{t\bar{t}} > 450\text{GeV})$	0.0336	-3.119	0.0968	-2.5614	0.1113	-2.434	0.1163	-2.389
$A_{FB}(M_{t\bar{t}} < 450\text{GeV})$	0.0453	-1.616	0.126	-1.3196	0.1446	-1.253	0.151	-1.23
$A_{FB}(\Delta Y > 1)$	0.0154	1.078	0.0282	1.1585	0.0285	1.1602	0.0284	1.159
$A_{FB}(\Delta Y < 1)$	0.0161	0.234	0.0358	0.3932	0.038	0.414	0.0391	0.420
χ^2		14.83		11.24		10.48		10.22
χ^2/ν		3.71		2.81		2.62		2.55
$ f_{13}^u $		0.549		1.319		2.105		2.905

TABLE II. Results of χ^2 analysis carried out for different values of m_{Σ_3} . The best fitted values for each observables along with their respective pulls are shown. The pull measures the deviation in the fitted value of the observable from its mean value. For NP contributions, the number of d.o.f. is 4 (No. of observables – No. of parameters.)

satisfy both the constraints for large range of coupling f_{13}^u within 1σ of the experimental bound.

The results of the χ^2 analysis are shown in Table II. We show the best-fit values of all the observables along with their respective pulls. The minimum values of χ^2 and the corresponding values of parameter f_{13}^u obtained at the minimum are shown for different masses of Σ_3 . The overall fits get better with increase in m_{Σ_3} . For all masses, we get the largest pulls corresponding to A_{FB} in the $M_{t\bar{t}} > 450$ GeV region where it gives more than 2σ deviation. All the other observables can be fitted within 1.2σ . Although the total χ^2 for

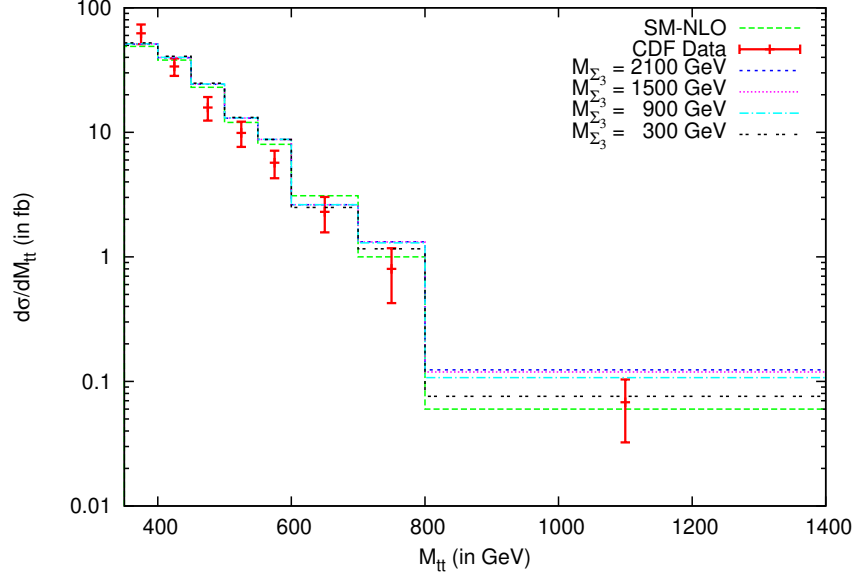


FIG. 5. The $t\bar{t}$ invariant mass distribution for NLO-SM, and for various masses of colored sextet Σ_3 for the best fitted values from our χ^2 analysis.

NP contribution is better than χ^2 for the SM, the χ^2/ν values are worse than the SM value for smaller values of Σ_3 mass. The χ^2/ν shows slight improvement relative to the SM only for masses greater than 1.5 TeV. Hence, the sextet Σ_3 in our model can satisfy the total cross section and the total asymmetry within 1σ while it is incompatible with asymmetries in the large invariant mass region and the large rapidity region for the same parameter space.

An empirical relation between f_{13}^u and m_{Σ_3} is obtained and can be written in approximate form as :

$$|f_{13}^u| = 0.148 + 1.31 \frac{m_{\Sigma_3}}{1 \text{ TeV}}. \quad (19)$$

Another important constraint in the $t\bar{t}$ production comes from the invariant mass distribution of $t\bar{t}$ pair. This distribution has been measured by CDF collaboration and is shown in Fig. 5 for various values of Σ_3 masses with CDF data and SM-NLO prediction. We use the best fit values of coupling f_{13}^u for various masses as shown in Table II for evaluating the contribution of NP to the $M_{t\bar{t}}$ distribution. The SM contribution to the $d\sigma/dM_{t\bar{t}}$ distribution in Fig. 5 has been evaluated to the full NLO order as given in Ref. [29]. While evaluating the contributions of NP and its interference with the SM to invariant $M_{t\bar{t}}$ distribution, we multiply the contribution with K-factor of 1.3. However, it is highly desirable to include full NLO corrections to NP to make more reliable prediction on the invariant mass distribution. We see that lower values of Σ_3 masses fit the distribution better than larger values of Σ_3 masses.

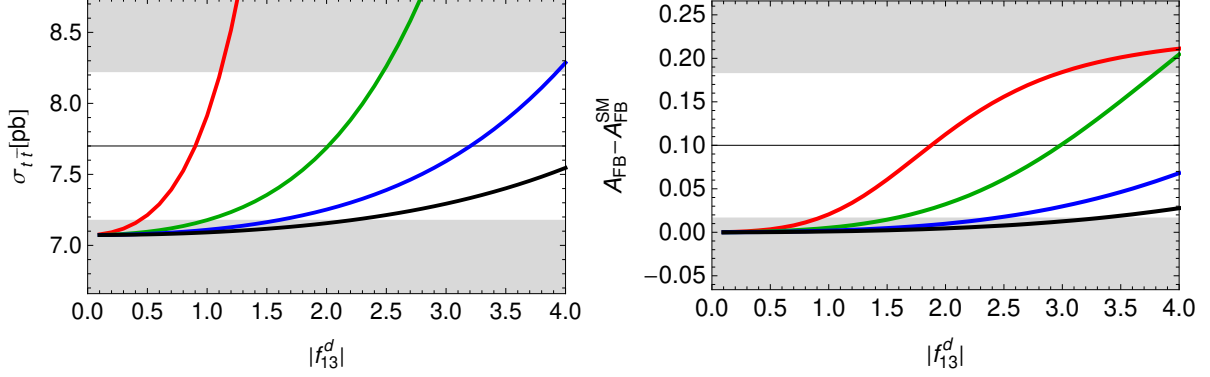


FIG. 6. The $t\bar{t}$ production cross section (left) and the forward backward asymmetry (right) as a function of the coupling f_{13}^d for masses $m_{\Sigma_4} = 300$ GeV (Red), 900 GeV (Green), 1500 GeV (Blue) and 2100 GeV (Black). The unshaded and the shaded region correspond to 1σ and 2σ experimental bounds respectively.

B. Diquark $(6, 1, \frac{1}{3})$

Next, we study the diquark Σ_4 to look at its effect on $t\bar{t}$ pair production at the Tevatron. The contribution of Σ_4 to $t\bar{t}$ production has been shown in Fig. 3 and proceeds through a $d\bar{d}$ initial state. In Fig. 6, we plot the cross section and the forward backward asymmetry for $t\bar{t}$ production at Tevatron as a function of coupling f_{13}^d for four different masses of colored sextet scalar Σ_4 . As stated earlier, in showing the contribution from new physics, we subtract the SM contribution from the experimentally measured value of A_{FB} .

Because of the fact that the PDF for the d-quark is smaller than that for the u-quark, we need larger values of the coupling f_{13}^d to generate the contribution to the observables of $t\bar{t}$ pair production. From Fig. 6, just like for Σ_3 , Σ_4 of mass 300 GeV can barely satisfy both $\sigma^{t\bar{t}}$ and A_{FB} for a very narrow range of coupling f_{13}^d that too at 2σ but with different range of coupling. For larger masses Σ_4 can satisfy both the constraints for large range of coupling f_{13}^d within 1σ of experimental bound but with a wider and different range of couplings as compared to Σ_3 .

The results of the χ^2 analysis for Σ_4 are shown in Table III. Similar to the previous case, the overall fits get better with increase in m_{Σ_4} . As seen earlier, the χ^2/ν values are worse than the SM value for smaller values of Σ_4 mass. Similar to the previous case, the best-fit relation between f_{13}^d and m_{Σ_4} can be put into approximate form as :

$$|f_{13}^d| = 0.273 + 2.48 \frac{m_{\Sigma_4}}{1 \text{ TeV}}. \quad (20)$$

The perturbativity argument regarding the strength of a generic coupling ‘ g ’ requires $g^2/4\pi < 1$, which allows, in principle, the coupling ‘ g ’ to be as large as ~ 3.5 . In Figs. 4 and 6, we show the cross section and the A_{FB} up to $f_{13}^{u,d} = 4$. However, these are not the canonical couplings which enter in the Lagrangian of Eq. 4. $f_{13}^{u,d}$ is related to the canonical

	$m_{\Sigma_4} = 300\text{GeV}$		$m_{\Sigma_4} = 900\text{GeV}$		$m_{\Sigma_4} = 1.5\text{TeV}$		$m_{\Sigma_4} = 2.1\text{TeV}$	
Observables	Fit	pull	Fit	pull	Fit	pull	Fit	pull
Cross section	8.0157	0.6071	8.2649	1.0863	8.2734	1.1027	8.2968	1.1478
A_{FB}	0.0230	-0.9277	0.0604	-0.4775	0.0490	-0.6143	0.0710	-0.3499
$A_{FB}(M_{t\bar{t}} > 450\text{GeV})$	0.0299	-3.1515	0.0985	-2.546	0.1041	-2.4972	0.1192	-2.3636
$A_{FB}(M_{t\bar{t}} < 450\text{GeV})$	0.0428	-1.6249	0.1299	-1.3070	0.1365	-1.2827	0.1547	-1.2164
$A_{FB}(\Delta Y > 1)$	0.0184	1.0971	0.0345	1.201	0.0338	1.1934	0.0350	1.2012
$A_{FB}(\Delta Y < 1)$	0.0173	0.2441	0.0405	0.4313	0.0405	0.4313	0.0429	0.4513
χ^2	15.07		11.23		11.09		10.15	
χ^2/ν	3.78		2.81		2.78		2.54	
$ f_{13}^d $	1.041		2.508		3.875		5.527	

TABLE III. Results of χ^2 analysis carried out for different values of m_{Σ_4} . The best fitted values for each observables along with their respective pulls are shown. The pull measures the deviation in the fitted value of the observable from its mean value. ν denote number of degree of freedom. For NP contributions, the number of degree of freedom is 4 (No. of observables – No. of parameters).

coupling F_{13} according to the Eq. 17. Using this relation, we find that the values of the couplings $f_{13}^{u,d}$ which we use in our analysis satisfy the perturbativity.

The invariant mass distribution of $t\bar{t}$ pair corresponding to contribution of Σ_4 is shown in Fig. 7 for various values of Σ_3 masses with CDF data and SM-NLO prediction. We use the best fit values of coupling f_{13}^d for various masses as shown in Table III for evaluating the contribution of NP to the $M_{t\bar{t}}$ distribution. From the fig., we see that all values of Σ_3 masses are more compatible with the distribution in the large $M_{t\bar{t}}$ bin and fit the distribution better than Σ_3 . However, there is a little tension in the distribution for bins 450 GeV-500 GeV and 550 GeV-600 GeV.

We now discuss the constraints on masses and couplings of the colored sextet Σ_3 and Σ_4 . These constraints have been discussed in detail in Ref. [30] where authors have analyzed the electroweak precision data (EWPD) to obtain lower bound on the mass of the sextet scalars. They find that EWPD does not give a lower bound much above 100 GeV. The constraint is weak because there is no custodial $SU(2)_c$ violation. The most robust bound on sextet masses comes from direct search of these scalars at LEP-II putting a lower limit of 105 GeV on their masses. At Tevatron, the most stringent bound comes [31] from the search of narrow resonances in the dijet mass spectrum. They reported lower mass bound for diquark to be 290 GeV. The Σ_3 can produce same sign dileptons through decay into two top quarks while Σ_4 safely avoids same sign dilepton constraints. The constraints on the mass of Σ_3 from the search of same sign dilepton signature is however weaker than the bound which comes from the search of narrow resonances.

The other stringent constraints come from low energy processes such as $D^0 - \bar{D}^0$ mixing. The contributions of the sextet colored scalars to this mixing has been studied in some detail

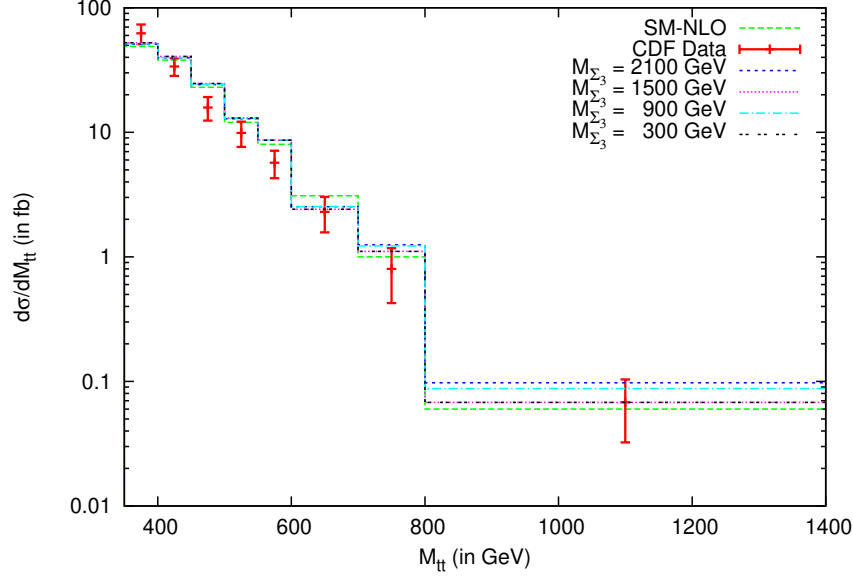


FIG. 7. The $t\bar{t}$ invariant mass distribution for NLO-SM, and for various masses of colored sextet Σ_4 for the best fitted values from our χ^2 analysis.

in Ref. [32]. Σ_3 contributes in $D^0 - \bar{D}^0$ mixing at tree level while Σ_4 contributes through a box diagram. The bound on parameter for the Σ_3 is $|Re(f_{22}^u f_{11}^{u*})| \lesssim 5.76 \times 10^{-7}$ for $m_H = 1$ TeV. The bound on coupling of Σ_4 is $|f_{12}^{d*} f_{11}^d|^2 \lesssim 1.7 \times 10^{-10}$ for $m_H = 1$ TeV. However, these bounds can be relaxed if the couplings to second generation is minimized which we do in our analysis for search these scalars at LHC.

IV. SEXTET DIQUARKS Σ_3 AND Σ_4 AT LHC

The detailed phenomenology of sextet diquarks has already been performed in Refs. [33–35] where they found that such scalars can be discovered at the LHC with masses around few GeV to 2 TeV. We have already shown in previous sections that Σ_3 and Σ_4 can have masses around this mass range in order to achieve unification at the GUT scale and explain the anomaly in the $t\bar{t}$ production forward backward asymmetry at Tevatron.

The colored sextet scalar diquarks can be produced in the following channels at LHC:

1. Resonant production in s-channel : $pp \rightarrow \Sigma_3/\Sigma_4 \rightarrow t + u/d + X$,
2. Pair-production : $pp \rightarrow \Sigma_3 \Sigma_3^*/\Sigma_4 \Sigma_4^* + X \rightarrow (t + u/d) + (\bar{t} + \bar{u}/\bar{d}) + X$,
3. Single production with top quarks : $pp \rightarrow \Sigma_{3,4} \bar{t}/\Sigma_{3,4}^* t + X$.

The channel 1 has been explored in detail in Refs. [33, 34]. The matrix amplitude squared and the resulting parton level cross section have been given in these references. The full NLO QCD corrections to $q\bar{q}$ annihilation to scalar sextet diquark resonant state has been

performed in Ref. [34]. In this channel, uu and ud initial states dominate over $\bar{u}\bar{u}$ and $\bar{u}\bar{d}$ initial states because of the large PDFs of quarks compared to antiquarks. Also, it is interesting to compare the cross sections corresponding to Σ_3 and Σ_4 production. The Σ_3 and Σ_4 get contributions from uu and ud initial state respectively. The Σ_3 gets enhancement due to large u -quark PDFs while Σ_4 gets enhancement from two sources : (a) due to combinatorics from initial state, the luminosity of Σ_4 is $du \otimes ud$ while that of Σ_3 is uu , and (b) from the relations 19 and 20, it can be seen that the coupling f_{13}^d is larger than f_{13}^u . Hence, the cross section for Σ_4 is almost 5 times larger than Σ_3 production cross section for low masses and is about 1.5 times larger for large values of Σ 's masses. The best strategy to discover $\Sigma_{3,4}$ in this channel would be to determine the invariant mass distribution of $\bar{t}+j$ and look for narrow resonances of $\Sigma_{3,4}$ as discussed in detail in Ref. [33].

The channel 2 has been explored in detail in Ref. [35]. The production process is mediated through QCD interactions through gg fusion and $q\bar{q}$ annihilation and hence depends only on sextet masses. The matrix amplitude squared and the resulting parton level cross section have been given in this reference. The channel in which Σ_3 decays to $t\bar{t}\bar{t}$ has been analyzed in great detail in Ref. [35] for 14 TeV LHC. They propose a reconstruction in the multijet plus same-sign dilepton with missing transverse energy samples to search for $t\bar{t}\bar{t}$ final states from sextet scalar production. The decays of Σ_4 would yield $(t+j) + (\bar{t}+j)$ which can be probed in 8-j channel of which two are b -jets and all jets are hard jets. The cross sections for both Σ_3 and Σ_4 are large enough so that they can be discovered in lower mass range at 14 TeV LHC. In Fig. 8, we show production cross sections for channel 1 and 2 for various cm energies of LHC and for various possible initial states. To calculate cross sections, we evaluate couplings f_{13}^u and f_{13}^d from relations 19 and 20 respectively and assume $f_{13}^u = f_{11}^u$ and $f_{13}^d = f_{11}^d$.

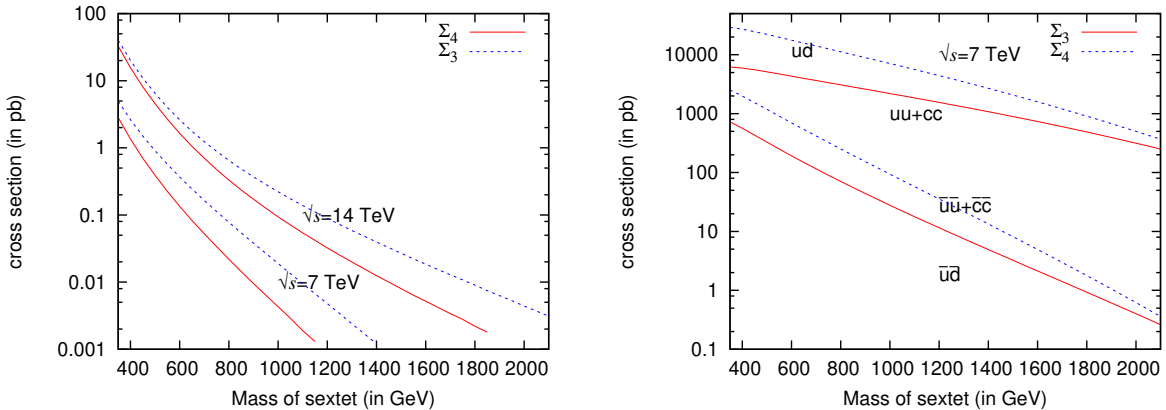


FIG. 8. The cross section for pair production $pp \rightarrow \Sigma_{3,4}\Sigma_{3,4}^* + X$ (left) and s-channel resonant production (right) of $pp \rightarrow \Sigma_{3,4} \rightarrow t+u/d+X$ with various initial states at the LHC. The values of the couplings f_{13}^u and f_{13}^d are evaluated using relation 19 and 20 respectively. We assume couplings $f_{13}^{d,u} = f_{11}^{d,u}$.

The Σ_3 and Σ_4 sextets can also be produced in association with antitop quarks. The cross sections for production of $\Sigma_3 + \bar{t}$ and $\Sigma_4 + \bar{t}$ pair have been shown in Fig. 9. Because

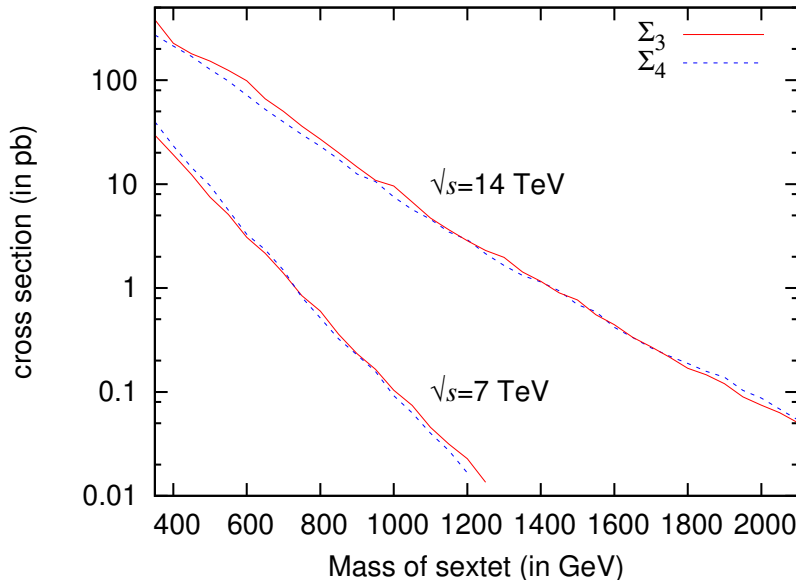


FIG. 9. The cross section for process $pp \rightarrow \Sigma_{3,4}\bar{t} + X$ at the LHC for two cm of energies. The values of the couplings f_{13}^u and f_{13}^d are evaluated using relation 19 and 20 respectively. We assume couplings $f_{13}^{d,u} = f_{11}^{d,u}$.

of the large couplings of Σ_4 , the cross section for Σ_4 production is comparable to that for Σ_3 production. We see that for the interesting mass range of the sextets, the cross section is of the order of SM $t\bar{t}$ cross section which makes this channel very promising. The search strategy in this channel would be to look for $t\bar{t}j$ final states and search for resonances in the invariant mass of light jet with antitop quark.

V. SUMMARY

In this paper, we have investigated the role of colored scalars as a possible explanation of large forward-backward asymmetry in $t\bar{t}$ pair production at Tevatron. We consider a particular non-supersymmetric $SO(10)$ model where such scalars reside in $\overline{126}$ dimensional scalar representation which plays a crucial part in GUT symmetry breaking and also generates small neutrino masses through seesaw mechanism. We find that either Σ_3 or Σ_4 colored sextet submultiplet of $\overline{126}$ can remain light and provide viable gauge coupling unification consistent with the present bounds on proton decay.

Colored scalars in the context of forward-backward asymmetry at Tevatron have been studied in Refs. [5, 7, 8]. All these papers are based on old CDF data and do not include new observations. In this paper, we show that the contributions of light colored sextet

scalars Σ_3 and Σ_4 of mass > 300 GeV can enhance the forward-backward asymmetry without spoiling the $\sigma(t\bar{t})$ and the invariant mass distribution. We perform a χ^2 analysis to simultaneously fit all the new observables along with total asymmetry and total cross section and find the best fitted values of the coupling for various masses. We find that all the observables can be fitted within 1.3σ of experiment errors except for the A_{FB} in $M_{t\bar{t}} > 450$ GeV region where we can fit the observation at 2.3σ . From the χ^2 analysis, we conclude that the colored sextet scalars of masses 1.5 TeV-2.1 TeV can provide a marginal improvement over the SM observations if all observations are simultaneously considered in the fit.

In this paper, we focus on the study of light colored sextet scalars in $SO(10)$ model and their effects to the A_{FB} in the light of new observations reported by CDF. We have shown that such scalars can emerge in particular $SO(10)$ model having masses of the order of TeV scale. However the detailed analysis carried out in context of new and old CDF data are applicable to any sextet scalar.

We also discuss the various production mechanisms of Σ_3 and Σ_4 at the LHC and find that these scalars will have observable cross section to be discovered in future. These scalars can be produced in pairs owing to pure QCD interactions and this channels is promising at LHC rather than Tevatron. They can also be produced in s-channel resonance and then can be probed in their decay to $t + j$ events. Also, the other promising channel is to search them in single production in association with anti top quarks. The best strategy to search for these scalars in all these channels would be to look for narrow resonance in invariant mass of top quarks with light jets.

Acknowledgements

We would like to thank Anjan S. Joshipura, Namit Mahajan and Saurabh D. Rindani for many useful discussions and suggestions at the different stages of this work and also for reading the manuscript. We also thank Sandip Pakvasa for useful discussion.

Note Added: While we were finishing the present work, Ref. [15] was appeared dealing with same kind of colored sextet state $(\bar{6}, 1, -\frac{4}{3})$. Our results for Σ_3 scalar qualitatively agree with their results. Compared to that work, we also study another sextet state and show that such scalars naturally emerge from theoretically well motivated $SO(10)$ model.

VI. APPENDIX

In this appendix, we list all the sub-multiplets of the $10(\phi)$, $\overline{126}(\Sigma)$ and $45(\chi)$ dimensional scalar representations of $SO(10)$ and their contributions to $B_{ij} = B_i - B_j$ coefficients (where B_i , $i = 1, 2, 3$ are one loop β function coefficients for $U(1)_Y$, $SU(2)_L$ and $SU(3)_c$ respectively). We also present these sub-multiplets in terms of their Pati-Salam subgroup $(SU(4) \times SU(2)_L \times SU(2)_R)$ notations. $(R-, R0, R+)$ represents components of the field which is triplet under $SU(2)_R$. The indices of the doublet of $SU(2)_L(SU(2)_R)$ are denoted

by $\alpha, \beta = 1, 2 (\alpha', \beta' = 1', 2')$. The index of the fundamental 4-plet of $SU(4)$ is denoted by $\mu(\nu) = \bar{\mu}(\bar{\nu}), 4$ where $\bar{\mu}, \bar{\nu} = 1, 2, 3$ represents the $SU(3)$ subgroup indices.

Fields ($SU(3), SU(2), Y$)	Pati-Salam Notations	ΔB_{23}	ΔB_{12}
$\phi_1(3, 1, -\frac{1}{3}), \bar{\phi}_1(\bar{3}, 1, \frac{1}{3})$	$\phi_{\bar{\mu}4}, \phi^{\bar{\mu}4}$	$-\frac{1}{6}$	$\frac{1}{15}$
$\phi_2(1, 2, \frac{1}{2}), \bar{\phi}_2(1, 2, -\frac{1}{2})$	$\phi_{\alpha 1'}, \phi_{2'}^\alpha$	$\frac{1}{6}$	$-\frac{1}{15}$
$\chi_1(8, 1, 0)$	$\chi_{\bar{\mu}}^{\bar{\nu}}$	$-\frac{1}{2}$	0
$\chi_2(3, 1, \frac{1}{3}), \bar{\chi}_2(\bar{3}, 1, -\frac{1}{3})$	$\chi_{\bar{\mu}}^4, \chi_4^{\bar{\nu}}$	$-\frac{1}{6}$	$\frac{1}{15}$
$\chi_{3,8}(1, 1, 0)$	$\chi^{(15)}, \chi^{(R0)}$	0	0
$\chi_4(3, 2, -\frac{5}{6}), \bar{\chi}_4(\bar{3}, 2, \frac{5}{6})$	$\chi_{\bar{\mu}4\alpha 2'}, \chi_{\bar{\mu}\bar{\nu}\alpha 1'}$	$\frac{1}{6}$	$\frac{1}{3}$
$\chi_5(3, 2, \frac{1}{6}), \bar{\chi}_5(\bar{3}, 2, -\frac{1}{6})$	$\chi_{\bar{\mu}4\alpha 1'}, \chi_{\bar{\mu}\bar{\nu}\alpha 2'}$	$\frac{1}{6}$	$-\frac{7}{15}$
$\chi_6(1, 3, 0)$	$\chi_{\alpha\beta}$	$\frac{1}{3}$	$-\frac{1}{3}$
$\chi_7(1, 1, 1), \bar{\chi}_7(1, 1, -1)$	$\chi^{(R+)}, \chi^{(R-)}$	0	$\frac{1}{5}$
$\Sigma_1(3, 1, -\frac{1}{3}), \bar{\Sigma}_1(\bar{3}, 1, \frac{1}{3})$	$\Sigma_{\bar{\mu}4}, \Sigma^{\bar{\mu}4}$	$-\frac{1}{6}$	$\frac{1}{15}$
$\Sigma_2(1, 2, \frac{1}{2}), \bar{\Sigma}_2(1, 2, -\frac{1}{2})$	$\Sigma_{\alpha 1'}, \Sigma_{2'}^\alpha$	$\frac{1}{6}$	$-\frac{1}{15}$
$\Sigma_3(6, 1, \frac{4}{3})$	$\Sigma_{\bar{\mu}\bar{\nu}}^{(R+)}$	$-\frac{5}{6}$	$\frac{32}{15}$
$\Sigma_4(6, 1, \frac{1}{3})$	$\Sigma_{\bar{\mu}\bar{\nu}}^{(R0)}$	$-\frac{5}{6}$	$\frac{2}{15}$
$\Sigma_5(6, 1, -\frac{2}{3})$	$\Sigma_{\bar{\mu}\bar{\nu}}^{(R-)}$	$-\frac{5}{6}$	$\frac{8}{15}$
$\Sigma_6(3, 1, \frac{2}{3})$	$\Sigma_{\bar{\mu}4}^{(R+)}$	$-\frac{1}{6}$	$\frac{4}{15}$
$\Sigma_7(3, 1, -\frac{1}{3})$	$\Sigma_{\bar{\mu}4}^{(R0)}$	$-\frac{1}{6}$	$\frac{1}{15}$
$\Sigma_8(3, 1, -\frac{4}{3})$	$\Sigma_{\bar{\mu}4}^{(R-)}$	$-\frac{1}{6}$	$\frac{1}{15}$
$\Sigma_9(1, 1, 0)$	$\Sigma_{44}^{(R+)}$	0	0
$\Sigma_{10}(1, 1, -1)$	$\Sigma_{44}^{(R0)}$	0	$\frac{1}{15}$
$\Sigma_{11}(1, 1, -2)$	$\Sigma_{44}^{(R-)}$	0	$\frac{1}{15}$
$\Sigma_{12}(\bar{6}, 3, -\frac{1}{3})$	$\Sigma_{\alpha\beta}^{\bar{\mu}\bar{\nu}}$	$\frac{3}{2}$	$-\frac{18}{5}$
$\Sigma_{13}(\bar{3}, 3, \frac{1}{3})$	$\Sigma_{\alpha\beta}^{\bar{\mu}4}$	$\frac{3}{2}$	$-\frac{9}{5}$
$\Sigma_{14}(1, 3, 1)$	$\Sigma_{\alpha\beta}^{44}$	$\frac{2}{3}$	$-\frac{1}{15}$
$\Sigma_{15}(8, 2, \frac{1}{2}), \bar{\Sigma}_{15}(8, 2, -\frac{1}{2})$	$\Sigma_{\bar{\mu}}^{\bar{\nu}}{}_{\alpha 1'}, \Sigma_{\bar{\mu}}^{\bar{\nu}}{}_{\alpha 2'}$	$-\frac{2}{3}$	$-\frac{8}{15}$
$\Sigma_{16}(3, 2, \frac{1}{6}), \bar{\Sigma}_{16}(\bar{3}, 2, -\frac{1}{6})$	$\Sigma_{\bar{\mu}}^4{}_{\alpha 2'}, \Sigma_4^{\bar{\nu}}{}_{\alpha 1'}$	$\frac{1}{6}$	$-\frac{7}{15}$
$\Sigma_{17}(3, 2, \frac{7}{6}), \bar{\Sigma}_{17}(\bar{3}, 2, -\frac{7}{6})$	$\Sigma_{\bar{\mu}}^4{}_{\alpha 1'}, \Sigma_4^{\bar{\nu}}{}_{\alpha 2'}$	$\frac{1}{6}$	$\frac{17}{15}$

TABLE IV. Different sub-multiplets of $10(\phi)$, $\overline{126}(\Sigma)$ and $45(\chi)$ dimensional scalar representations of $SO(10)$ and their contribution to B_{ij} coefficients of Eq. 6. Various notations used are explained in text.

[1] T. Aaltonen *et al.* [CDF Collaboration], Phys. Rev. Lett. **101**, 202001 (2008) [arXiv:0806.2472 [hep-ex]].

- [2] V. M. Abazov *et al.* [D0 Collaboration], Phys. Rev. Lett. **100**, 142002 (2008) [arXiv:0712.0851 [hep-ex]].
- [3] M. T. Bowen, S. D. Ellis and D. Rainwater, Phys. Rev. D **73**, 014008 (2006) [arXiv:hep-ph/0509267];
O. Antunano, J. H. Kuhn and G. Rodrigo, Phys. Rev. D **77**, 014003 (2008) [arXiv:0709.1652 [hep-ph]];
L. G. Almeida, G. F. Sterman and W. Vogelsang, Phys. Rev. D **78**, 014008 (2008) [arXiv:0805.1885 [hep-ph]].
- [4] P. H. Frampton, J. Shu and K. Wang, Phys. Lett. B **683**, 294 (2010) [arXiv:0911.2955 [hep-ph]];
J. Cao, Z. Heng, L. Wu and J. M. Yang, Phys. Rev. D **81**, 014016 (2010) [arXiv:0912.1447 [hep-ph]];
K. Cheung, W. Y. Keung and T. C. Yuan, Phys. Lett. B **682**, 287 (2009) [arXiv:0908.2589 [hep-ph]];
B. Xiao, Y. k. Wang and S. h. Zhu, Phys. Rev. D **82**, 034026 (2010) [arXiv:1006.2510 [hep-ph]];
M. Bauer, F. Goertz, U. Haisch, T. Pfoh and S. Westhoff, JHEP **1011**, 039 (2010) [arXiv:1008.0742 [hep-ph]];
C. H. Chen, G. Cvetcic and C. S. Kim, Phys. Lett. B **694**, 393 (2011) [arXiv:1009.4165 [hep-ph]];
A. Djouadi, G. Moreau, F. Richard and R. K. Singh, Phys. Rev. D **82**, 071702 (2010) [arXiv:0906.0604 [hep-ph]];
E. Alvarez, L. Da Rold and A. Szyrkman, arXiv:1011.6557 [hep-ph];
D. W. Jung, P. Ko and J. S. Lee, arXiv:1011.5976 [hep-ph];
J. Cao, L. Wang, L. Wu and J. M. Yang, arXiv:1101.4456 [hep-ph];
D. Choudhury, R. M. Godbole, S. D. Rindani and P. Saha, arXiv:1012.4750 [hep-ph];
E. L. Berger, Q. H. Cao, C. R. Chen, C. S. Li and H. Zhang, arXiv:1101.5625 [hep-ph];
V. Barger, W. Y. Keung and C. T. Yu, Phys. Rev. D **81**, 113009 (2010) [arXiv:1002.1048 [hep-ph]];
S. Jung, H. Murayama, A. Pierce and J. D. Wells, Phys. Rev. D **81**, 015004 (2010) [arXiv:0907.4112 [hep-ph]].
- [5] J. Shu, T. M. P. Tait and K. Wang, Phys. Rev. D **81**, 034012 (2010) [arXiv:0911.3237 [hep-ph]].
- [6] D. W. Jung, P. Ko, J. S. Lee and S. h. Nam, Phys. Lett. B **691**, 238 (2010) [arXiv:0912.1105 [hep-ph]].
- [7] A. Arhrib, R. Benbrik and C. H. Chen, Phys. Rev. D **82**, 034034 (2010) [arXiv:0911.4875 [hep-ph]].
- [8] I. Dorsner, S. Fajfer, J. F. Kamenik *et al.*, Phys. Rev. D **81**, 055009 (2010). [arXiv:0912.0972 [hep-ph]].
- [9] I. Dorsner, S. Fajfer, J. F. Kamenik and N. Kosnik, Phys. Rev. D **82**, 094015 (2010) [arXiv:1007.2604 [hep-ph]].

- [10] T. Aaltonen *et al.* [CDF Collaboration], arXiv:1101.0034 [hep-ex].
- [11] T. Aaltonen *et al.* [CDF Collaboration], Phys. Rev. Lett. **105**, 012001 (2010) [arXiv:1004.3224 [hep-ex]].
- [12] MCFM stands for Monte Carlo for FeMtobarn processes: <http://mcfm.fnal.gov/>
- [13] T. Aaltonen *et al.* [CDF Collaboration], Phys. Rev. Lett. **102**, 222003 (2009) [arXiv:0903.2850 [hep-ex]].
- [14] K. Cheung and T. C. Yuan, arXiv:1101.1445 [hep-ph];
C. Delaunay, O. Gedalia, S. J. Lee, G. Perez and E. Ponton, arXiv:1101.2902 [hep-ph];
V. Barger, W. Y. Keung and C. T. Yu, arXiv:1102.0279 [hep-ph];
B. Bhattacharjee, S. S. Biswal and D. Ghosh, arXiv:1102.0545 [hep-ph].
- [15] B. Grinstein, A. L. Kagan, M. Trott and J. Zupan, arXiv:1102.3374 [hep-ph].
- [16] H. Georgi and C. Jarlskog, Phys. Lett. B **86**297 (1979).
- [17] S. Bertolini, L. Di Luzio and M. Malinsky, Phys. Rev. D **80**, 015013 (2009) [arXiv:0903.4049 [hep-ph]];
S. Bertolini, L. Di Luzio and M. Malinsky, Phys. Rev. D **81**, 035015 (2010) [arXiv:0912.1796 [hep-ph]].
- [18] A. S. Joshipura and K. M. Patel, arXiv:1102.5148 [hep-ph].
- [19] R. N. Mohapatra and B. Sakita, Phys. Rev. D **21**, 1062 (1980).
- [20] F. Wilczek and A. Zee, Phys. Rev. D **25**, 553 (1982).
- [21] C. S. Aulakh and A. Girdhar, Nucl. Phys. B **711**, 275 (2005) [arXiv:hep-ph/0405074];
C. S. Aulakh and A. Girdhar, Int. J. Mod. Phys. A **20**, 865 (2005) [arXiv:hep-ph/0204097];
P. Nath and R. M. Syed, Phys. Lett. B **506**, 68 (2001) [Erratum-ibid. B **508**, 216 (2001)] [arXiv:hep-ph/0103165];
T. Fukuyama, A. Ilakovac, T. Kikuchi, S. Meljanac and N. Okada, Eur. Phys. J. C **42**, 191 (2005) [arXiv:hep-ph/0401213];
T. Fukuyama, A. Ilakovac, T. Kikuchi, S. Meljanac and N. Okada, J. Math. Phys. **46**, 033505 (2005) [arXiv:hep-ph/0405300].
- [22] T. P. Cheng, E. Eichten and L. F. Li, Phys. Rev. D **9**, 2259 (1974).
- [23] A. Giveon, L. J. Hall and U. Sarid, Phys. Lett. B **271**, 138 (1991).
- [24] C. Amsler *et al.* [Particle Data Group Collaboration], Phys. Lett. **B667**, 1-1340 (2008).
- [25] H. Nishino *et al.* [Super-Kamiokande Collaboration], Detector,” Phys. Rev. Lett. **102**, 141801 (2009). [arXiv:0903.0676 [hep-ex]].
- [26] R. N. Mohapatra and G. Senjanovic, Phys. Rev. D **27**, 1601 (1983).
- [27] J. Pumplin, A. Belyaev, J. Huston, D. Stump and W. K. Tung, JHEP **0602**, 032 (2006) [arXiv:hep-ph/0512167].
- [28] N. Kidonakis and R. Vogt, Phys. Rev. D **78**, 074005 (2008) [arXiv:0805.3844 [hep-ph]].
- [29] Q. H. Cao, D. McKeen, J. L. Rosner, G. Shaughnessy and C. E. M. Wagner, Phys. Rev. D **81**, 114004 (2010) [arXiv:1003.3461 [hep-ph]].

- [30] J. M. Arnold, M. Pospelov, M. Trott and M. B. Wise, JHEP **1001**, 073 (2010) [arXiv:0911.2225 [hep-ph]].
- [31] T. Aaltonen *et al.* [CDF Collaboration], Phys. Rev. D **79**, 112002 (2009) [arXiv:0812.4036 [hep-ex]].
- [32] C. H. Chen, Phys. Lett. B **680**, 133 (2009) [arXiv:0902.2620 [hep-ph]].
- [33] R. N. Mohapatra, N. Okada and H. B. Yu, Phys. Rev. D **77**, 011701 (2008) [arXiv:0709.1486 [hep-ph]], E. L. Berger, Q. H. Cao, C. R. Chen, G. Shaughnessy and H. Zhang, Phys. Rev. Lett. **105**, 181802 (2010) [arXiv:1005.2622 [hep-ph]],
- [34] T. Han, I. Lewis and T. McElmurry, JHEP **1001**, 123 (2010) [arXiv:0909.2666 [hep-ph]].
- [35] C. R. Chen, W. Klemm, V. Rentala and K. Wang, Phys. Rev. D **79**, 054002 (2009) [arXiv:0811.2105 [hep-ph]].